Journal of Pathology
J Pathol 2017
Published online in Wiley Online Library
(wileyonlinelibrary.com) DOI: 10.1002/path.4977

ORIGINAL PAPER

PTEN loss and activation of K-RAS and β-catenin cooperate to accelerate prostate tumourigenesis

Matthew T Jefferies[1,2†], Adam C Cox[1,3†], Boris Y Shorning[1], Valerie Meniel[1], David Griffiths[4], Howard G Kynaston[2,5], Matthew J Smalley[1*] and Alan R Clarke[1]

[1] *The European Cancer Stem Cell Research Institute, School of Biosciences, Cardiff University, Cardiff, UK*
[2] *Institute of Cancer and Genetics, Cardiff University School of Medicine, Cardiff, UK*
[3] *Department of Urology, Morriston Hospital, Swansea, UK*
[4] *Department of Pathology, University Hospital of Wales, Cardiff, UK*
[5] *Department of Urology, University Hospital of Wales, Cardiff, UK*

**Correspondence to: Matthew J Smalley, The European Cancer Stem Cell Research Institute, School of Biosciences, Cardiff University, Hadyn Ellis Building, Maindy Road, Cardiff, CF24 4HQ, UK. E-mail: smalleymj@cardiff.ac.uk*

[†]Equal contributions.

Abstract

Aberrant phosphoinositide 3-kinase (PI3K), mitogen-activated protein kinase (MAPK) and WNT signalling are emerging as key events in the multistep nature of prostate tumourigenesis and progression. Here, we report a compound prostate cancer murine model in which these signalling pathways cooperate to produce a more aggressive prostate cancer phenotype. Using Cre-LoxP technology and the *probasin* promoter, we combined the loss of *Pten* (*Pten*$^{fl/fl}$), to activate the PI3K signalling pathway, with either dominant stabilized β-catenin [*Catnb*$^{+/lox(ex3)}$] or activated K-RAS (*K-Ras*$^{+/V12}$) to aberrantly activate WNT and MAPK signalling, respectively. Synchronous activation of all three pathways (triple mutants) significantly reduced survival (median 96 days) as compared with double mutants [median: 140 days for *Catnb*$^{+/lox(ex3)}$*Pten*$^{fl/fl}$; 182 days for *Catnb*$^{+/lox(ex3)}$*K-Ras*$^{+/V12}$; 238 days for *Pten*$^{fl/fl}$*K-Ras*$^{+/V12}$], and single mutants [median: 383 days for *Catnb*$^{+/lox(ex3)}$; 407 days for *Pten*$^{fl/fl}$], reflecting the accelerated tumourigenesis. Tumours followed a stepwise progression from mouse prostate intraepithelial neoplasia to invasive adenocarcinoma, similar to that seen in human disease. There was significantly elevated cellular proliferation, tumour growth and percentage of invasive adenocarcinoma in triple mutants as compared with double mutants and single mutants. Triple mutants showed not only activated AKT, extracellular-signal regulated kinase 1/2, and nuclear β-catenin, but also significantly elevated signalling through mechanistic target of rapamycin complex 1 (mTORC1). In summary, we show that combined deregulation of the PI3K, MAPK and WNT signalling pathways drives rapid progression of prostate tumourigenesis, and that deregulation of all three pathways results in tumours showing aberrant mTORC1 signalling. As mTORC1 signalling is emerging as a key driver of androgen deprivation therapy resistance, our findings are important for understanding the biology of therapy-resistant prostate cancer and identifying potential approaches to overcome this.

Keywords: prostate cancer; *Pten*; *K-Ras*; β-catenin; WNT, mTORC1

Received 28 January 2017; Revised 15 August 2017; Accepted 22 August 2017

No conflicts of interest were declared.

Introduction

Advanced molecular and genetic technologies have identified a vast number of somatic mutations, copy number alterations and oncogenic structural DNA rearrangements in both primary [1–5] and metastatic prostate cancer (PCa) [6–10]. However, these studies, together with the COSMIC database (http://cancer.sanger.ac.uk/cosmic), highlight a limited number of highly recurrent abnormalities in specific genes/pathways. Recurrent somatic mutations in cell signalling pathways or processes that can be clinically actionable/targeted by emerging therapies include, for example, mutations in the WNT, phosphoinositide 3-kinase (PI3K) and mitogen-activated protein kinase (MAPK) signalling pathways.

Deregulation of WNT signalling is implicated in many cancers. The best known example is colorectal cancer; >90% of colorectal cancers have an activating mutation of the canonical WNT signalling pathway [11]. In PCa, deregulated WNT signalling has been investigated primarily in metastatic disease, with somatic alteration of the adenomatous polyposis coli (APC) tumour suppressor gene and the β-catenin gene having been reported in 8.7–19.7% and 4.9–12% of cases, respectively [7,10]. WNT signalling has

also been implicated in the lethal phase of PCa, i.e. castration-resistant prostate cancer (CRPC), independently of androgen signalling [6,7]. Upregulation of the PI3K pathway, encompassing multiple somatic alterations such as deletion/mutations in PTEN, PI3K, or AKT, has been reported in 42% of primary tumours and 100% of metastatic tumours [1], suggesting that this pathway plays a key role in the ability of the cancer cell to metastasize. Finally, aberrations that result in upregulation of the MAPK pathway are also common in PCa, with pathway alterations having been reported in 43% of primary tumours and 90% of metastases [1]. The MAPK signalling pathway has been implicated not only in the initial phase of metastasis but also in the late transition to CRPC [12].

Historically, signalling pathways have been studied as linear entities that do not interact; however, the importance of pathway crosstalk that results in complex signalling webs is now understood. There is a growing appreciation that this crosstalk is key for tumour development and progression. We have previously shown in the mouse that the WNT and MAPK pathways synergize to accelerate prostate tumourigenesis [13]. Others have demonstrated that canonical WNT signalling promotes prostate carcinogenesis driven by fibroblast growth factor receptor 1 [which activates both the PI3K pathway and the MEK–extracellular-signal regulated kinase (ERK) pathway] [14]. Crosstalk between the WNT and PI3K pathways in prostate tumourigenesis has been shown previously [15], and several studies have investigated synergistic effects of the PI3K and MAPK pathways in mouse models [16–19]. The mechanisms of c-MYC activation also suggest a possible convergence between the WNT, PI3K and MAPK pathways in PCa. *c-Myc* is an important WNT target gene and a key effector of deregulated WNT signalling [20], although it can also be activated in a WNT-independent manner, as demonstrated in a murine PCa model of *Pten* deletion and mutant B-RAF activation [17].

We hypothesized that combined deregulation of PI3K, WNT and MAPK signalling could cooperate to accelerate prostate tumourigenesis. To test this, we used an *in vivo* genetics approach to combine aberrant PI3K, WNT and MAPK signalling in the mouse prostate [13]. We report here that, whereas activating any two of these pathways together accelerates tumourigenesis more than single-pathway activation, combining all three further augments tumour formation, indicating that each pathway makes a distinct contribution to the process of tumourigenesis. Furthermore, we observed the strongest mechanistic target of rapamycin complex 1 (mTORC1) activation in triple mutants, consistent with findings from a human PCa tissue microarray (TMA), suggesting that this may be the target of the synergistic activity of these three pathways. As mTORC1 signalling is emerging as a key driver of resistance to androgen deprivation therapy (ADT), and stimulates tumour growth in the setting of castrate levels of testosterone, our findings are important for understanding the biology of therapy-resistant PCa and identifying potential approaches to overcome this.

Materials and methods

Experimental animals

All animal studies, including breeding, were carried out under UK Home Office regulations following local ethical approval and according to the ARRIVE guidelines [21]. *Probasin* (*Pb*)-*Cre4* mice were sourced from the Mouse Models of Human Cancer Consortium (National Cancer Institute, Frederick, MD, USA). The alleles used in this study were β-*catenin*$^{+/lox(ex3)}$ [22], *K-Ras*$^{+/V12}$ [23], and *Pten*$^{fl/fl}$ [24]. The *Pb-Cre4* transgene was incorporated into cohorts by the use of male mice, because *Pb-Cre4*-positive female mice have been shown to recombine floxed alleles in the ovaries, resulting in a mosaic phenotype [25]. Mice were genotyped from DNA isolated from ear nicks. Each *loxP*-targeted allele and the Cre-recombinase transgene were detected as described previously [22–24]. Kaplan–Meier (KM) survival analysis was carried out with GraphPad Prism (Version 5.0b). Only mice that reached specified endpoints when euthanasia was necessary because of prostate disease were included in KM curves.

In some cases, bromodeoxyuridine (BrdU) (GE Healthcare, Cardiff, UK) was administered by intraperitoneal injection; mice were killed 2 h after administration.

Tissue isolation and histology

Tissue was harvested and fixed in 10% neutral buffered formaldehyde at 4 °C for no more than 24 h. Samples were embedded in paraffin, sectioned at 5 µm, and stained with haematoxylin and eosin (H&E) for histological analysis. To assess the severity or aggressiveness of the tumour histologically, the percentage of invasion was estimated at 100 days and at the endpoint (death or 500 days).

Histological analysis of the prostate gland was performed in accordance with the consensus report from the New York meeting of the Mouse Models of Human Cancer Consortium prostate pathology committee [26]. The histological subtype descriptors used were mouse prostate intraepithelial neoplasia (mPIN), microinvasive adenocarcinoma, and invasive adenocarcinoma.

Immunohistochemistry, TMA analysis, and western blotting

Standard immunohistochemistry and western blotting techniques were used throughout this study. TMAs of human prostate samples were approved under the Human Tissue Act and Welsh Cancer Bank (WCB), project number 12/007. Full details of the antibodies used and dilutions, staining quantification methods (Quickscore) and TMA analysis are provided in supplementary material, Supplementary materials and methods.

Results

WNT, PI3K and MAPK signalling are elevated in human PCa and are associated with the mTORC1 pathway

A number of studies have suggested the importance of WNT, PI3K and MAPK signalling in the initiation, progression and metastasis of human PCa [1,6,7,10–12], and TMA analysis has previously shown simultaneous activation of PI3K–AKT and RAS–MAPK signalling in patients with late-stage prostate disease [16–19]. To assess the interaction between these pathways and to help identify a pathway of potential convergence, we analysed human PCa by using a WCB TMA of 317 samples: 244 prostate adenocarcinomas and 73 benign controls. We found significant upregulation of markers associated with activation of all three pathways (WNT, PI3K and MAPK signalling) in PCa as compared with benign controls (Figure 1A–C). Furthermore, when samples were separated on the basis of no/mild staining and moderate/strong staining for the downstream mTORC1 marker phospho-S6 (p-S6), there was a clear correlation between p-S6 staining and activation of all three pathways (Figure 1D, E). Our data therefore suggest that mTORC1 signalling may act as a convergence point for these three pathways.

Pten loss and activation of K-RAS and β-catenin (triple mutants) cooperate to accelerate prostate tumourigenesis

To test the hypothesis that mTORC1 signalling in PCa requires simultaneous activation of the WNT, PI3K and MAPK pathways, we used an *in vivo* genetics approach. We generated eight cohorts of *Pb-Cre4*-positive mice carrying different combinations of conditional alleles for *Pten* loss ($Pten^{fl/fl}$) and for β-catenin [$Catnb^{+/lox(ex3)}$] and K-RAS ($K\text{-}Ras^{+/V12}$) activation. These were subdivided into three groups according to their genotype: four 'singles' [wild-type (WT), $Pten^{fl/fl}$, $Catnb^{+/lox(ex3)}$, and $K\text{-}Ras^{+/V12}$], three 'doubles' [$Catnb^{+/lox(ex3)}K\text{-}Ras^{+/V12}$, $Pten^{fl/fl}K\text{-}Ras^{+/V12}$, $Catnb^{+/lox(ex3)}Pten^{fl/fl}$], and a 'triple' [$Catnb^{+/lox(ex3)}Pten^{fl/fl}K\text{-}Ras^{+/V12}$]. Fifteen mice from each cohort were aged until they reached specified endpoints or 500 days, whichever was sooner. Additional mice were humanely killed for histological and western blotting analysis at 100 days ($n=6$) and at time points of 70, 100, 200, 250 ($Pten^{fl/fl}K\text{-}Ras^{+/V12}$ only), 300, 350 ($Pten^{fl/fl}$ only) and 400 days to weigh prostates, in order to estimate increasing tumour burden over time ($n=3$).

All WT and $Pb\text{-}Cre4^{+}K\text{-}Ras^{+/V12}$ single mutants survived until the end of the experiment (500 days). As reported previously [13], and similarly to what has been seen when $K\text{-}Ras^{+/D12}$ is expressed alone [16–19], $K\text{-}Ras^{+/V12}$ mice did not develop PCa, with all mice surviving to the end of the experiment (500 days). All other mouse models developed extensive invasive adenocarcinoma of the prostate (100% incidence), resulting in ureteric or bladder outflow obstruction secondary to the local effects of the primary tumour. Consistent with reports from others [13,27], activation of β-catenin ($Pb\text{-}Cre4^{+}Catnb^{+/ex3}$) or homozygous deletion of *Pten* ($Pb\text{-}Cre4^{+}Pten^{fl/fl}$) resulted in reduced median survival times of 383 days (range 339–476 days) and 407 days (range 350–479 days), respectively (Figure 1F).

All double mutants had reduced survival as compared with single mutants ($P<0.0001$, log-rank) (Figure 1F). Mice with activation of both β-catenin and K-RAS ($Pb\text{-}Cre4^{+}Catnb^{+/ex3}K\text{-}Ras^{+/V12}$) had a median survival of 182 days (range 170–208 days), as reported previously [13]. Mice with loss of *Pten* and activation of β-catenin ($Pb\text{-}Cre4^{+}Catnb^{+/ex3}Pten^{fl/fl}$) had a median survival of 140 days (range 109–181 days). Mice with both *Pten* loss and activation of K-RAS ($Pb\text{-}Cre4^{+}Pten^{fl/fl}K\text{-}Ras^{+/V12}$) had a median survival that was reduced to 238 days (range 200–292 days, $P<0.0001$, log-rank; this is longer than in models using the more aggressive $K\text{-}Ras^{+/D12}$: 20-week and 40-week median survival have been reported for $Pten^{fl/fl}K\text{-}Ras^{+/D12}$ and $Pten^{+/fl}K\text{-}Ras^{+/D12}$, respectively) [16–19]. However, triple mutants with *Pten* loss in addition to activation of β-catenin and K-RAS ($Pb\text{-}Cre4^{+}Catnb^{+/ex3}Pten^{fl/fl}K\text{-}Ras^{+/V12}$) showed significantly earlier morbidity and mortality than double mutants, with a median survival of 96 days ($n=15$; range 76–130 days, $P<0.0001$, log-rank) (Figure 1F).

Tumour progression occurs in a stepwise fashion similar to that of human disease from mPIN to invasive adenocarcinoma

All tumour models examined showed stepwise progression from mPIN to microinvasive and invasive adenocarcinoma (Figure 2) as the cohorts aged (as shown by analysis of mice at time points between days 70 and 400).

Histologically normal prostates from WT mice (Figure 2A–C) showed avid androgen receptor (AR) staining of luminal epithelial cells as well as some stromal reactivity (Figure 2B), and possessed an intact basal layer as confirmed by positive cytokeratin (CK) 5 staining (Figure 2C). mPIN was characterized by increased cell proliferation within the glands with frequent cellular atypia (Figure 2D). There was positive nuclear AR staining (Figure 2E) of the luminal cells, and positive membranous CK5 staining of the basal layer (Figure 2F). Lesions were classified as microinvasive adenocarcinoma when the normal glandular structure showed distortions with some epithelial cells invading into the surrounding stroma (typically <1 mm). At the site of such invasion, there was a breach in the basal layer with local loss of the basal cell marker CK5 but positive AR staining of the cells invading the stroma (Figure 2G–I). Similarly to human PCa, invasive adenocarcinoma of mouse prostate showed widespread loss of CK5 positivity, and the whole basal layer was breached, allowing invasion of epithelial cells into the stroma (Figure 2J–L; supplementary material, Figure S1A–C). Tumours were

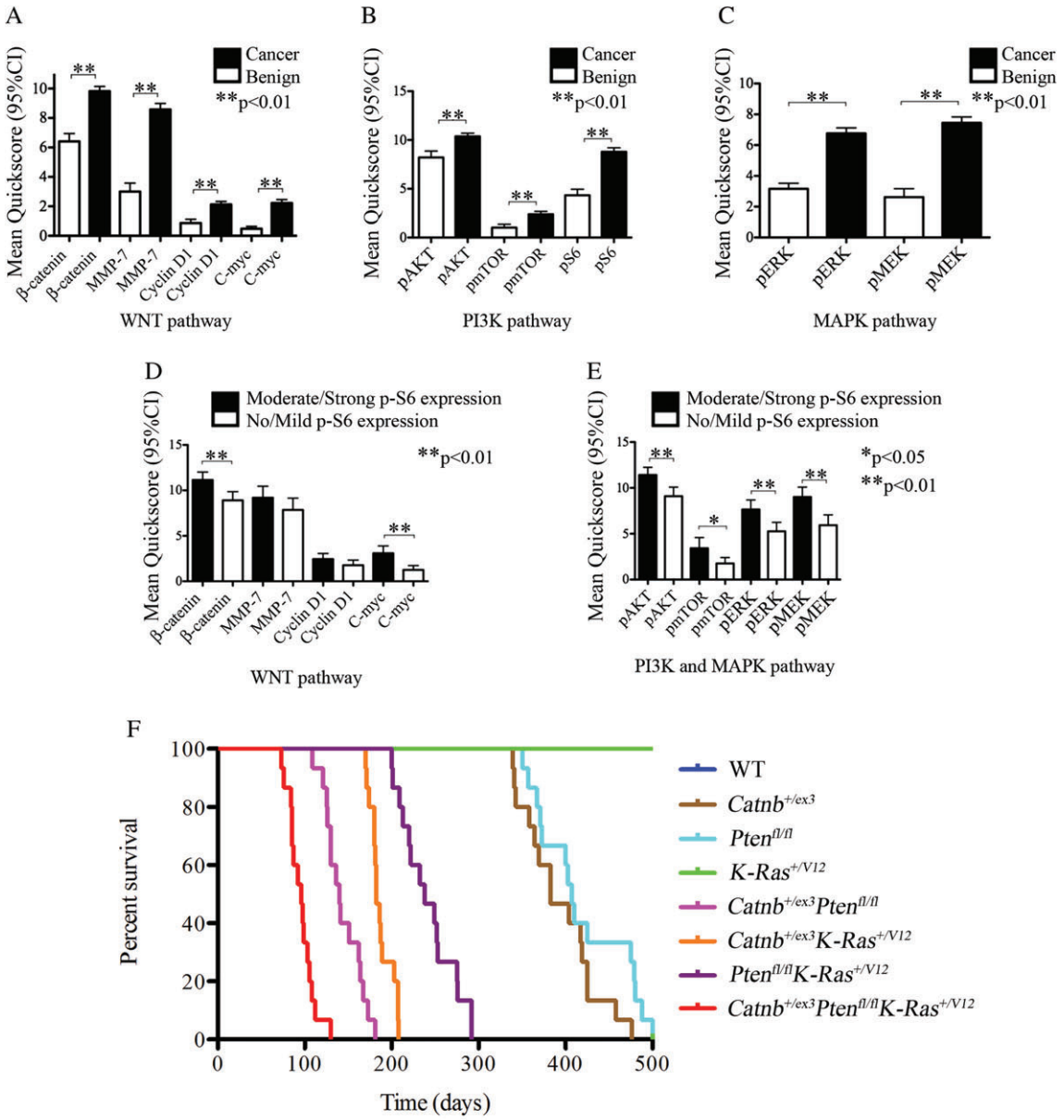

	WT	*Pten*$^{fl/fl}$	*Catn*$^{+/ex3}$	*K-Ras*$^{+/V12}$	*Catn*$^{+/ex3}$ *K-Ras*$^{+/V12}$	*Pten*$^{fl/fl}$ *K-Ras*$^{+/V12}$	*Catn*$^{+/ex3}$ *Pten*$^{fl/fl}$
Pten$^{fl/fl}$	p<0.0001						
Catn$^{+/ex3}$	p<0.0001	p<0.0001					
K-Ras$^{+/V12}$	N.S. (p=1)	N.S. (p=0.104)	p<0.0001				
Catn$^{+/ex3}$ *K-Ras*$^{+/V12}$	p<0.0001	p<0.0001	p<0.0001	p<0.0001			
Pten$^{fl/fl}$ *K-Ras*$^{+/V12}$	p<0.0001	p<0.0001	p<0.0001	p<0.0001	p<0.0001		
Catn$^{+/ex3}$ *Pten*$^{fl/fl}$	p<0.0001	p<0.0001	p<0.0001	p<0.0001	p<0.0001	p<0.0001	
Catn$^{+/ex3}$ *Pten*$^{fl/fl}$ *K-Ras*$^{+/V12}$	p<0.0001	p<0.0001	p<0.0001	p<0.0001	p<0.0001	p<0.0001	p<0.0001

Figure 1. Immunohistochemistry for WNT, PI3K, MAPK and mTOR pathway markers in a human PCa TMA, and KM survival curves for *in vivo* genetic models. (A–C) Immunohistochemistry for expression of markers of WNT (A), PI3K (B) and MAPK (C) pathway activation in human PCa TMAs, demonstrating higher activity (as assessed by mean Quickscore) in cancer than in benign prostatic tissue. (D) Assessment of WNT pathway activation marker staining as a function of p-S6 staining (no/mild versus moderate/strong staining, using mean Quickscore), demonstrating positive correlation of nuclear β-catenin and c-MYC with increased p-S6 staining. (E) Assessment of PI3K and MAPK pathway activation marker staining as function of p-S6 staining, demonstrating positive correlation of all markers (p-AKT, p-mTOR, p-ERK and p-MEK) with increased p-S6 staining. Error bars represent mean with 95% confidence interval (CI), unpaired *t*-test: $^{*}P < 0.05$, $^{**}P < 0.01$. (F) KM survival curves for mouse models (top) and statistical analysis (bottom). The median survival for triple mutants (*Pb-Cre4*$^{+}$ *Catnb*$^{+/ex3}$ *Pten*$^{fl/fl}$ *K-Ras*$^{+/V12}$) was significantly lower than that for double mutants ($P < 0.0001$, log-rank): 96 days (range 76–130 days), as compared with 238 days (range 200–292 days), 182 days (range 170–208 days) and 140 days (range 109–181 days) for the double mutants: *Pb-Cre4*$^{+}$ *Pten*$^{fl/fl}$ *K-Ras*$^{+/V12}$, *Pb-Cre4*$^{+}$ *Catnb*$^{+/ex3}$ *K-Ras*$^{+/V12}$ and *Pb-Cre4*$^{+}$ *Catnb*$^{+/ex3}$ *Pten*$^{fl/fl}$, respectively. All double mutant combinations had significantly shorter survival than single mutants ($P < 0.0001$, log-rank). The survival times of *Pb-Cre4*$^{+}$ *Catnb*$^{+/ex3}$ and *Pb-Cre4*$^{+}$ *Pten*$^{fl/fl}$ were 383 days (range 339–476 days) and 407 days (range 350–479 days), respectively. *Pb-Cre4*$^{+}$ *K-Ras*$^{+/V12}$ and WT mice all survived to the endpoint of the experiment (500 days). MMP, matrix metalloproteinase.

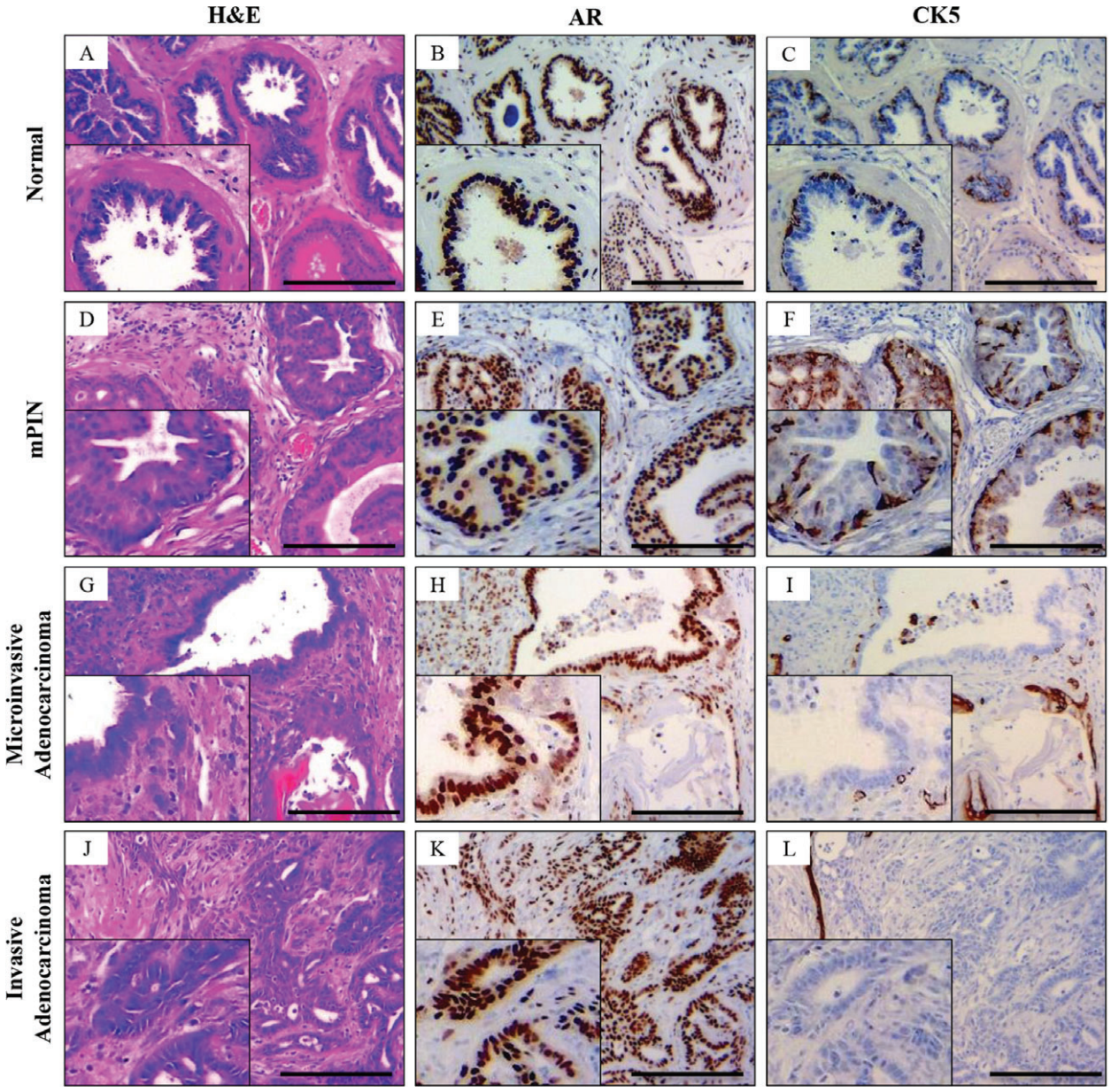

Figure 2. Histological characterization of normal prostate gland, mPIN, microinvasive adenocarcinoma, and diffuse adenocarcinoma of the mouse prostate. (A) H&E staining of the histologically normal prostate gland. (B and C) AR immunohistochemistry demonstrates avid staining of the luminal cells (B), with CK5 staining the membrane of the basal layer abutting the basement membrane in a continuous fashion (C). (D) mPIN has a characteristic appearance with increased cell proliferation in the glands, with frequent cellular atypia. (E and F) mPIN lesions show widespread AR staining (E), whereas CK5 staining remains continuous (F). (G and H) In microinvasive adenocarcinoma (G), the glandular structure begins to distort, with focal areas of microinvasion of AR-positive (H) epithelial cells into the surrounding stroma. (I) At the site of invasion, there is loss of the continuous CK5 staining basal layer. (J) H&E staining of prostate adenocarcinoma sections demonstrates diffuse invasion of epithelial cells into the stroma, with fusion of glands and areas of cribriform pattern, which is pathognomonic of human Gleason pattern 4. (K) AR staining demonstrates intensely stained epithelial cells invading the stroma with loss of the basal marker CK5 (L). Scale bars: 200 μm. Insets magnified two-fold.

rapidly proliferating with frequent mitoses and rare apoptotic bodies (supplementary material, Figure S1A, B). As the tumours progressed, the prostate glandular architecture became increasingly distorted as glands fused together and areas of cribriform pattern formed, pathognomonic of Gleason pattern 4 (Figure 2J; supplementary material, Figure S1B). Furthermore, features of Gleason pattern 5 developed, with single PCa cells appearing in the stroma (supplementary material, Figure S1C).

All tumour models investigated showed reactive stroma and regions with mesenchymal morphology (spindle-shaped cells that can be classified as sarcomatoid metaplasia) adjacent to epithelial areas with mPIN and invasive adenocarcinoma (supplementary material, Figure S1D). Abnormal differentiation was evident from regions staining for both epithelial [pan-CK (pCK)] and mesenchymal (vimentin) immunohistochemical markers (supplementary material, Figure S1E, F).

In all models in which a mutated β-catenin allele was present, squamous metaplasia characterized by epithelial-like tumour cells acquiring a squamous morphology and focal areas of hyperkeratinization ('keratin pearls'; supplementary material, Figure S1G) were common, consistent with previous observations in mouse PCa models with activated WNT [13,15,28–31]. Areas of squamous metaplasia stained strongly for the basal keratin CK5 (supplementary material, Figure S1H), in contrast to prostate adenocarcinoma (Figure 2L).

Combinatorial pathway mutations shift the spectrum of lesions to a more aggressive phenotype

To compare the progression of disease between different mouse models, we assessed the percentage of invasive adenocarcinoma in each mouse cohort at a fixed time point of 100 days (supplementary material, Figure S2). As expected, WT and single *K-Ras*$^{+/V12}$ mutant mice had histologically normal prostates at this time. Single *Catnb*$^{+/ex3}$ and *Pten*$^{fl/fl}$ mice, and *Catnb*$^{+/lox(ex3)}$*K-Ras*$^{+/V12}$ mice, showed areas of mPIN but no invasion at 100 days. *Pten*$^{fl/fl}$*K-Ras*$^{+/V12}$ and *Catnb*$^{+/lox(ex3)}$*Pten*$^{fl/fl}$ double mutants predominantly showed mPIN with areas of microinvasive adenocarcinoma at 100 days (particularly the latter cohort), whereas triple mutants had widespread invasive adenocarcinoma. To assess the rate of growth of tumours, tumour burden was estimated by weighing prostates of mice killed at 70, 100, 200, 250 (*Pten*$^{fl/fl}$*K-Ras*$^{+/V12}$ only), 300, 350 (*Pten*$^{fl/fl}$ only) and 400 days (supplementary material, Figure S3). Prostate weights in *Catnb*$^{+/ex3}$*Pten*$^{fl/fl}$*K-Ras*$^{+/V12}$ triple mutants increased rapidly from the earliest time point; *Catnb*$^{+/lox(ex3)}$*Pten*$^{fl/fl}$ prostates showed a similar behaviour. The other cohorts showed either a delay before tumour growth or little or no increase in prostate weight at all (in the WT and *K-Ras*$^{+/V12}$ mice; supplementary material, Figure S3). These growth patterns were reflected by proliferation within tumours as analysed by Ki67 staining and BrdU labelling (supplementary material, Figure S4). Triple mutants had a significantly higher percentage of Ki67-positive cells than all other genotypes at 100 days. By the experimental endpoint, proliferation in the triple mutants (as determined by either Ki67 staining or BrdU labelling) was still significantly higher than in the WT and all of the single mutant cohorts. However, proliferation in the double mutants at their endpoints was similar to that of the triple mutants at their endpoint [the differences in proliferation at endpoint between *Pten*$^{fl/fl}$*K-Ras*$^{+/V12}$ and *Catnb*$^{+/ex3}$*Pten*$^{fl/fl}$*K-Ras*$^{+/V12}$ mice determined by Ki67 staining, and between *Catnb*$^{+/lox(ex3)}$*Pten*$^{fl/fl}$ and *Catnb*$^{+/ex3}$*Pten*$^{fl/fl}$*K-Ras*$^{+/V12}$ mice determined by BrdU labelling, being not significant; supplementary material, Figure S4]. The rate of apoptosis was low (<1%) across all tumours, with no significant differences between genotypes (supplementary material, Figure S5).

Triple mutants therefore had faster-growing tumours with a more aggressive histological phenotype and an increased amount of invasive adenocarcinoma, resulting in significantly reduced survival as compared with double and single mutants.

Both K-Ras and β-catenin mutations drive metastatic spread in the context of loss of Pten

To assess metastatic potential in the mouse, retroperitoneal lymph nodes were harvested for each genotype and assessed histologically for metastasis (Figure 3). We observed metastatic deposits in only two cohorts: 10% ($n = 1/10$) of *Catnb*$^{+/ex3}$*Pten*$^{fl/fl}$ and 60% ($n = 6/10$) of *Pten*$^{fl/fl}$*K-Ras*$^{+/V12}$ double mutants showed nodal metastasis (supplementary material, Table S1). All metastatic lymph nodes examined had areas of neoplastic prostatic epithelium located at the capsule of the node, with fusion of glands and a cribriform pattern (Figure 3A), morphologically similar to that seen in the corresponding prostate tumour specimens and strongly positive for pCK (Figure 3B).

Triple mutation perturbs the 'checks and balances' of mechanistic target of rapamycin (mTOR) signalling regulation in mouse prostate

To assess whether the accelerated rate of tumour formation and rapid progression in the triple mutants was due to a synergistic effect between the WNT, PI3K–AKT–mTOR and MAPK pathways, we assessed β-catenin levels and localization, and key readouts of the PI3K–AKT–mTOR and MAPK pathways, in prostate tissue of all cohorts by semiquantitative immunohistochemistry on aged mice (Figures 4 and 5; supplementary material, Figures S6 and S7) and western blotting on 100-day-old mice (Figure 6; supplementary material, Figure S8).

Localization of β-catenin in aged mice was primarily at the cell membrane in prostates of WT, *Pten*$^{fl/fl}$, *K-Ras*$^{+/V12}$ and *Pten*$^{fl/fl}$*K-Ras*$^{+/V12}$ mutant mice (Figure 4A, D, J, M; Figure 5D), although some nuclear localization was observed (Figure 4N). Nuclear localization of β-catenin in *Pten*$^{fl/fl}$*K-Ras*$^{+/V12}$ mice was largely associated with invasive areas (Figure 5D), possibly because of relocalization from cell membranes of invading cells after E-cadherin loss [32]. In single mutants, double mutants and triple mutants expressing *Catnb*$^{+/ex3}$, there was a significant increase in nuclear localization of β-catenin (Figure 4G, N; Figure 5A, G, J), but there was less β-catenin nuclear staining in cohorts in which *Pten* had been knocked out but β-catenin was WT (Figure 4N; supplementary material, Table S2). Overall β-catenin levels as measured at 100 days were largely stable (Figure 6; supplementary material, Figure S8), possibly because of negative feedback loops regulating WNT signalling [33,34], but, in mice carrying a mutant *K-Ras*$^{+/V12}$ but WT β-catenin, we observed a > 2-fold decrease in total β-catenin levels (relative levels of β-catenin: WT = 1, *K-Ras*$^{+/V12}$ = 0.44,

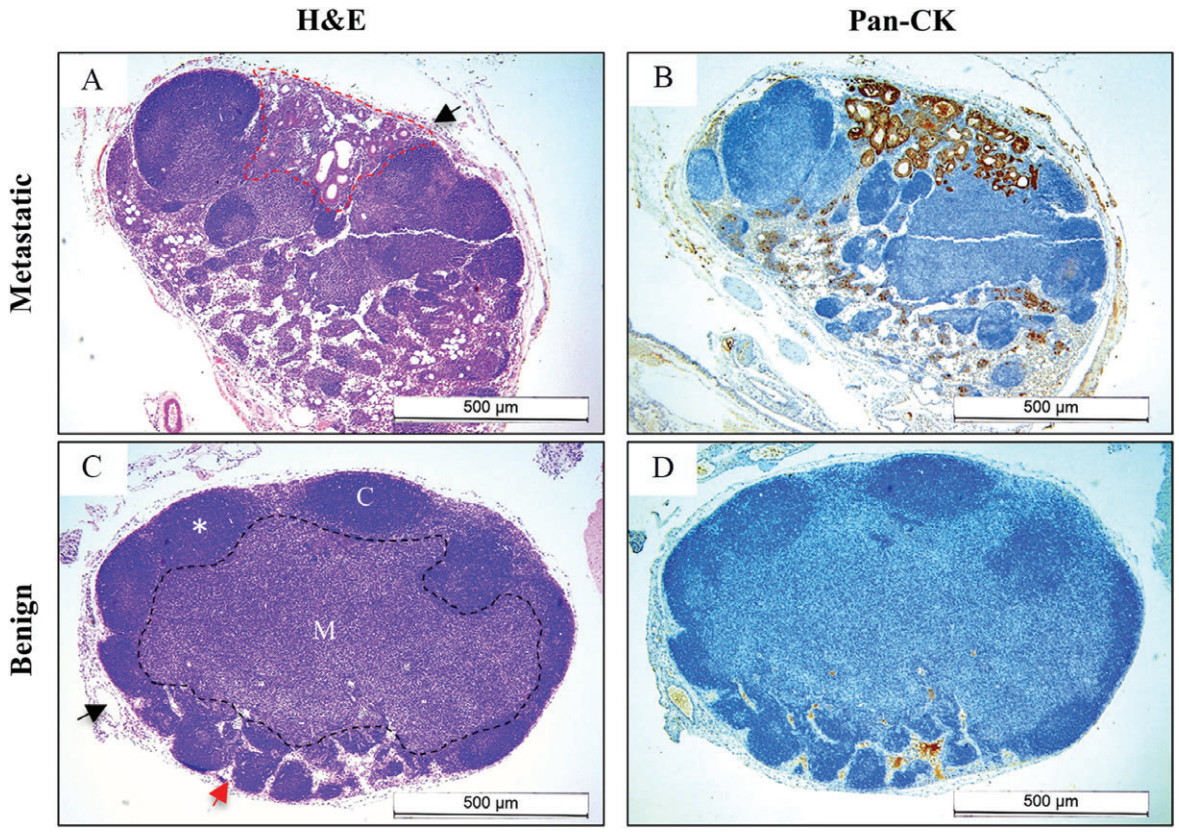

Figure 3. Lymph node characterization. (A) Metastatic prostate epithelium extending from the capsule (black arrow) and infiltrating into the node (red dotted line). (B) Metastatic node staining avidly for pCK. (C) Benign reactive node with the inner medulla (M) and outer cortex (C) separated by the dotted black line. The capsule and marginal sinus (black arrow) surround the node, with the cortex separated by cortical sinuses (red arrow). Germinal centre within the cortex of the node (*). (D) Minimal non-specific pCK staining in a benign node. Scale bars as indicated.

$P < 0.05$; $Pten^{fl/fl}K\text{-}Ras^{+/V12} = 0.43$, $P = 0.05$; Figure 6; supplementary material, Figure S8).

AKT activation by phosphorylation at both regulatory residues was present at 100 days in all cohorts with *Pten* ablation and, to a lesser extent, in $Catnb^{+/ex3}K\text{-}Ras^{+/V12}$ mice (relative levels of p-AKT^{Thr308}: WT = 1, $Pten^{fl/fl} = 13.89$, $Pten^{fl/fl}K\text{-}Ras^{+/V12} = 14.88$, $Pten^{fl/fl}Catnb^{+/ex3} = 6.04$, $Catnb^{+/ex3}K\text{-}Ras^{+/V12} = 1.89$, $Catnb^{+/ex3}Pten^{fl/fl}K\text{-}Ras^{+/V12} = 7.62$; p-AKT^{Ser473}: WT = 1, $Pten^{fl/fl} = 12.76$, $Catnb^{+/ex3}K\text{-}Ras^{+/V12} = 2.90$, $Catnb^{+/ex3}Pten^{fl/fl} = 16.72$, $Pten^{fl/fl}K\text{-}Ras^{+/V12} = 20.53$, $Catnb^{+/ex3}Pten^{fl/fl}K\text{-}Ras^{+/V12} = 9.36$; for all comparisons, $P < 0.01$ relative to WT; Figure 6; supplementary material, Figure S8). This was confirmed by p-AKT^{Thr308} staining of aged prostates (Figure 4B, E, H, K and Figure 5B, E, H, K, M; supplementary material, Table S1).

AKT is known to inhibit glycogen synthase kinase 3β (GSK3β) activity by phosphorylating Ser9 [35], which can serve as readout of AKT activity. Although GSK3β is a part of the β-catenin destruction complex, AKT-dependent Ser9 phosphorylation is not likely to affect WNT signalling, but rather tuberous sclerosis complex (TSC) 1/2 [36]. Phospho-GSK3β^{Ser9} (p-GSK3β^{Ser9}) levels in prostates from aged mice (supplementary material, Figure S6) largely correlated with AKT activation, with staining being detected only in cohorts with deleted *Pten* and in $Catnb^{+/ex3}K\text{-}Ras^{+/V12}$ mice (supplementary material, Figure S6). Prostates from the $Catnb^{+/ex3}Pten^{fl/fl}$ and $Catnb^{+/ex3}Pten^{fl/fl}K\text{-}Ras^{+/V12}$ cohorts had significantly higher levels of p-GSK3β^{Ser9} than all other cohorts (supplementary material, Figure S6H, I).

Total levels of phospho-ERK1/2 (p-ERK1/2) (p44/42 MAPK) were lower in 100-day-old $K\text{-}Ras^{+/V12}$ mice and all other tumour models than in age-matched WT mice as determined by western blotting (WT = 1, $K\text{-}Ras^{+/V12} = 0.27$, $P < 0.01$; Figure 6; supplementary material, Figure S8). Although these findings are surprising at face value, the ERK signalling network has numerous negative feedback loops [37], and, when *Pten* was deleted and β-catenin was activated, $K\text{-}Ras^{+/V12}$ expression led to a 7.2-fold increase in p-ERK1/2 levels ($Catnb^{+/ex3}Pten^{fl/fl}K\text{-}Ras^{+/V12}$ versus $Catnb^{+/ex3}Pten^{fl/fl}$, $P < 0.01$; Figure 6; supplementary material, Figure S8), although this still did not fully restore WT levels. However, immunostaining of aged prostates for p-ERK1/2 revealed that, whereas WT mice tended to have moderate, uniform staining, tumour models were more heterogeneous, with areas of focal strong staining that cannot be distinguished in western blots (supplementary material, Figure S7). Indeed, by Quickscore, aged WT and $K\text{-}Ras^{+/V12}$ mice had similar levels of p-ERK1/2,

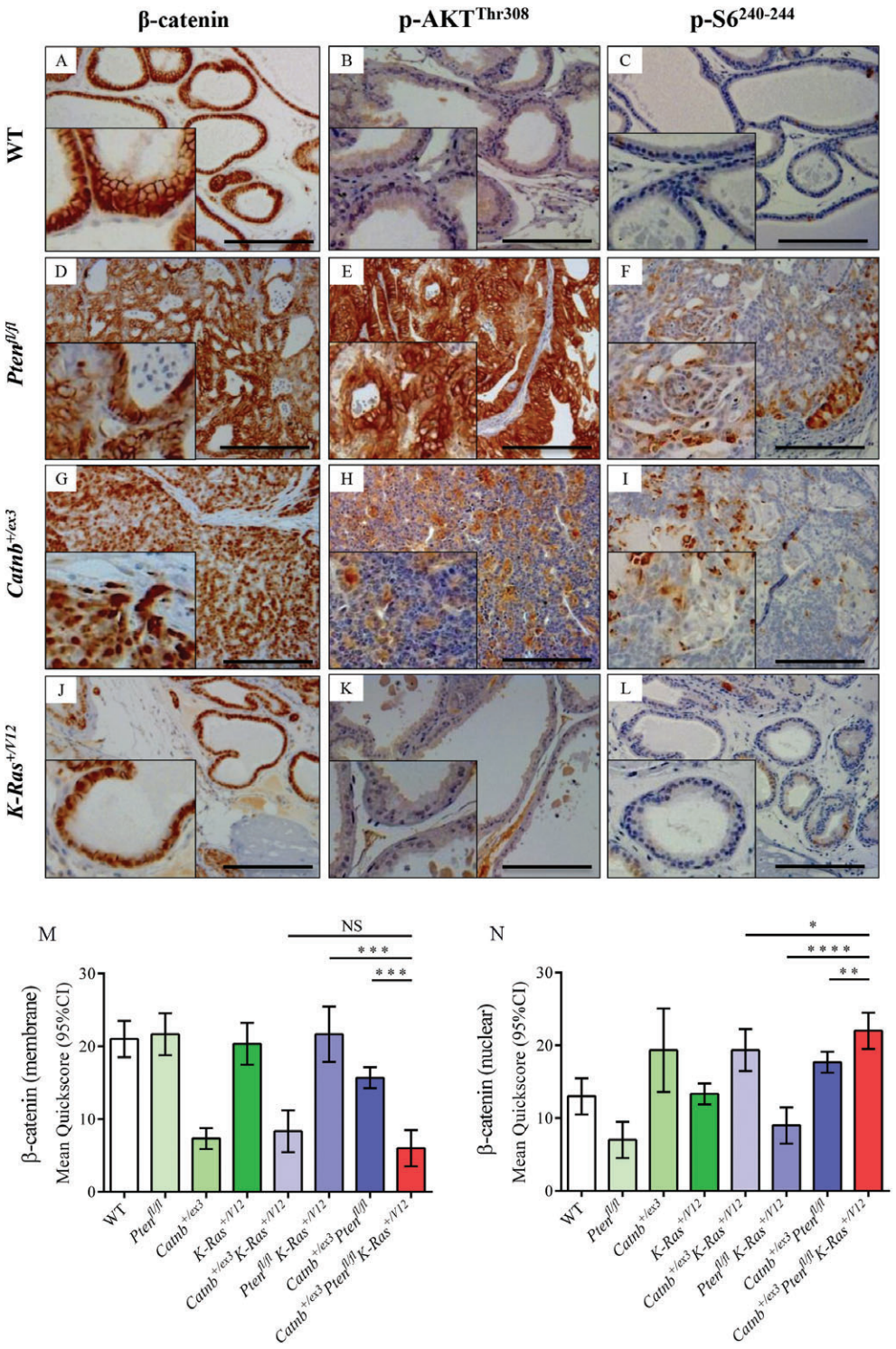

Figure 4. Immunohistochemistry for β-catenin, p-AKT^{Thr308} and p-S6$^{240-244}$ in WT and single allele mouse models. (A–L) Immunostaining with antibodies against β-catenin (A, D, G, and J), p-AKT^{Thr308} (B, E, H, and K), and p-S6$^{240-244}$ (C, F, I, and L) on WT (A–C), *Pb-Cre4*$^{+}$ *Pten*$^{fl/fl}$ (D–F), *Pb-Cre4*$^{+}$ *Catnb*$^{+/ex3}$ (G–I) and *Pb-Cre4*$^{+}$ *K-Ras*$^{+/V12}$ (I and J) cohorts of mice ($n = 4$) at the endpoint of the experiment (500 days or when sick). Scale bars: 200 μm. Insets are magnified two-fold. (M and N) Quickscore quantification of β-catenin membrane-specific (M) and nuclear (N) staining in all genotypes, including the staining presented in Figure 5. Note: Quickscore quantification of p-AKT^{Thr308} and p-S6$^{240-244}$ for all genotypes is shown in Figure 5M, N. For clarity, the significance of Quickscore staining in triple mutant versus double mutant cohorts only is presented on the graphs (*$P < 0.05$; **$P < 0.01$; ***$P < 0.001$; unpaired two-tailed *t*-test, $n = 4$); full statistical comparisons of all genotypes are given in supplementary material, Table S1. WT prostates showed predominantly membranous staining for β-catenin, with some nuclear staining, but no p-AKT^{Thr308} or p-S6$^{240-244}$ reactivity (A–C). *Pten*$^{fl/fl}$ tumours had membranous staining for β-catenin, rare nuclear positivity, diffuse staining for p-AKT^{Thr308}, and focal staining for p-S6$^{240-244}$ (D–F). *Catnb*$^{+/ex3}$ tumours had strong nuclear staining for β-catenin, with reduced cell membrane staining, and focal positive staining for p-AKT^{Thr308} and p-S6$^{240-244}$ (G–I). *K-Ras*$^{+/V12}$ tumours had predominantly membranous staining for β-catenin with some nuclear positivity and no staining for p-AKT^{Thr308} or p-S6$^{240-244}$ (J–L). CI, confidence interval; NS, not significant.

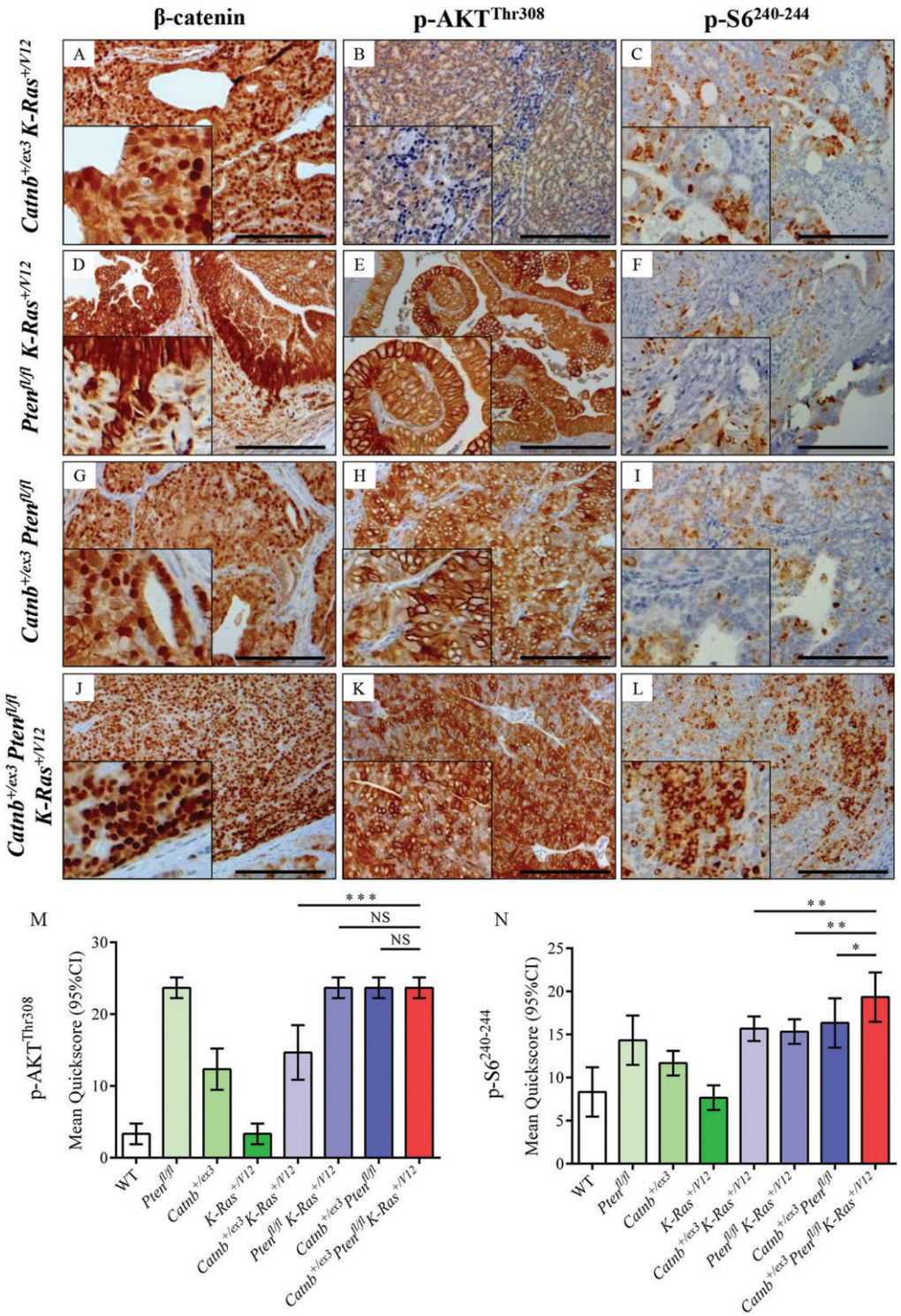

Figure 5. Immunohistochemistry for β-catenin, p-AKT^{Thr308} and p-S6$^{240-244}$ in double and triple allele mouse models. (A–L) Immunostaining for β-catenin (A, D, G, and J), p-AKT^{Thr308} (B, E, H, and K) and p-S6$^{240-244}$ (C, F, I, and L) on *Pb-Cre4*$^{+}$ *Catnb*$^{+/ex3}$ *K-Ras*$^{+/V12}$ (A–C), *Pb-Cre4*$^{+}$ *Pten*$^{fl/fl}$ *K-Ras*$^{+/V12}$ (D–F), *Pb-Cre4*$^{+}$ *Catnb*$^{+/ex3}$ *Pten*$^{fl/fl}$ (G–I) and *Pb-Cre4*$^{+}$ *Catnb*$^{+/ex3}$ *Pten*$^{fl/fl}$ *K-Ras*$^{+/V12}$ (J–L) cohorts of mice ($n = 4$) at the endpoint of the experiment (500 days or when sick). Scale bars: 200 μm. Insets are magnified two-fold. (M and N) Quickscore quantification of p-AKT^{Thr308} and p-S6$^{240-244}$ for all genotypes. For Quickscore quantification of β-catenin membrane-specific staining (M) and nuclear staining (N), see Figure 4M, N. For clarity, the significance of Quickscore staining in triple mutant versus double mutant cohorts only is presented on the graphs (*$P < 0.05$; **$P < 0.01$; ***$P < 0.001$; unpaired two-tailed *t*-test, $n = 4$); full statistical comparisons of all genotypes are given in supplementary material, Table S1. *Catnb*$^{+/ex3}$ *K-Ras*$^{+/V12}$ tumours showed predominantly nuclear staining for β-catenin, with weak focal staining for p-AKT^{Thr308} and p-S6$^{240-244}$ (A–C). *Pten*$^{fl/fl}$ *K-Ras*$^{+/V12}$ tumours had strong membranous staining for β-catenin, strong diffuse staining for p-AKT^{Thr308}, and focal positive staining for p-S6$^{240-244}$ (D–F). *Catnb*$^{+/ex3}$ *Pten*$^{fl/fl}$ tumours showed both nuclear and membrane-specific β-catenin staining, diffuse staining for p-AKT^{Thr308}, and focal positive staining for p-S6$^{240-244}$ (G-I). *Catnb*$^{+/ex3}$ *Pten*$^{fl/fl}$ *K-Ras*$^{+/V12}$ tumours stained avidly for nuclear β-catenin, and showed diffuse strong staining for both p-AKT^{Thr308} and p-S6$^{240-244}$ (J–L), the latter being significantly higher than in all other cohorts. CI, confidence interval; NS, not significant.

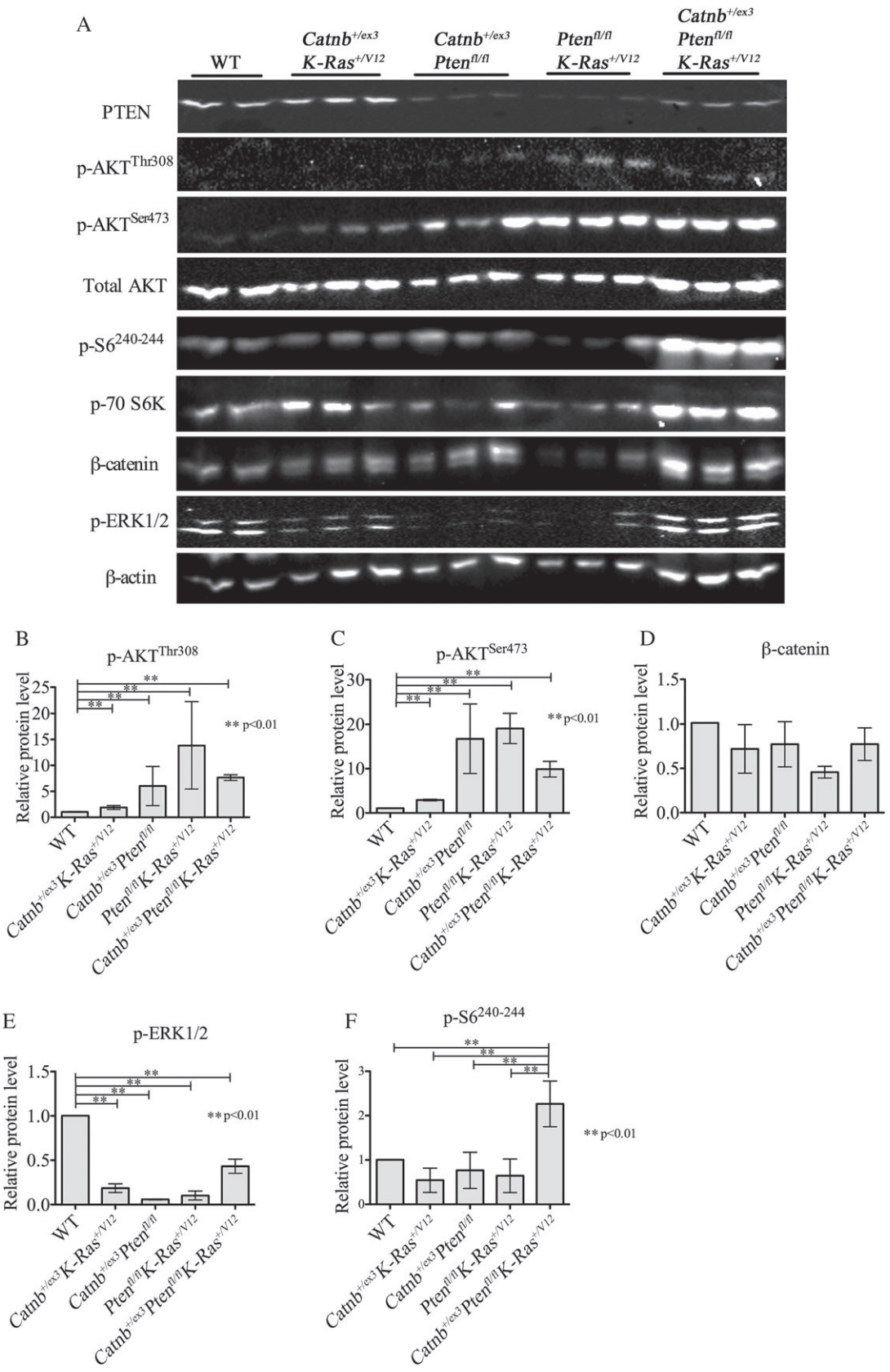

Figure 6. Biochemical analysis of signalling pathways in prostate tissue from double and triple allele models. (A) Western blot analysis of markers of activation of the PI3K, WNT, MAPK and mTOR signalling pathways for WT, double mutants ($Catnb^{+/ex3}K\text{-}Ras^{+/V12}$, $Pten^{fl/fl}Catnb^{+/ex3}$, and $Pten^{fl/fl}K\text{-}Ras^{+/V12}$) and triple mutants ($Catnb^{+/ex3}Pten^{fl/fl}K\text{-}Ras^{+/V12}$). Protein was extracted from fresh frozen prostate tissue from 100-day-old mice for each cohort ($n=3$). The following antibodies were used: the PI3K pathway markers PTEN, p-AKT^{Thr308}, p-AKT^{Ser473}, and total AKT; the WNT pathway marker β-catenin; the MAPK pathway marker p-ERK1/2; and the mTOR pathway markers p-70S6 K and p-S6$^{240-244}$. β-Actin was used as a loading reference. (B–F) Relative quantification of p-AKT^{Thr308} (B), pAKT^{Ser473} (C), β-catenin (D), p-ERK1/2 (E) and p-S6$^{240-244}$ (F). Error bars: mean with 95% confidence interval. *$P < 0.05$, **$P < 0.01$, unpaired two-tailed t-test, $n=3$.

and all other models had significantly higher p-ERK1/2 levels (supplementary material, Figure S7I).

Finally, ribosomal protein S6 phosphorylation is a key readout of mTORC1 activity [38]. Western blot analysis of younger (100-day-old) mice revealed that only $Catnb^{+/ex3}Pten^{fl/fl}K\text{-}Ras^{+/V12}$ mice showed significantly increased levels of p-S6$^{240-244}$ (WT = 1, $Catnb^{+/ex3}K\text{-}Ras^{+/V12} = 0.49$, $Catnb^{+/ex3}Pten^{fl/fl} = 0.69$, $Pten^{fl/fl}K\text{-}Ras^{+/V12} = 0.47$, $Catnb^{+/ex3}Pten^{fl/fl}K\text{-}Ras^{+/V12} = 2.09$, $P < 0.01$; Figure 6; supplementary material, Figure S8). This three-fold to four-fold increase in p-S6$^{240-244}$ levels observed in the triple mutants as compared with the double mutants suggests the abrogation of negative feedback loops controlling mTORC1. Furthermore, prostate tissue from aged $Catnb^{+/ex3}Pten^{fl/fl}K\text{-}Ras^{+/V12}$ mice also had significantly higher levels of p-S6$^{240-244}$ than prostate tissue from aged mice of other genotypes ($P < 0.05$ as compared with the next closest genotype; Figure 4C, F, I, L and Figure 5C, F, I, L, N).

Therefore, our study supports the hypothesis that mTORC1 signalling in PCa requires simultaneous activation of the WNT, PI3K and MAPK pathways, as suggested by the human TMA data, and that this results in a more aggressive tumour phenotype. Furthermore, it suggests that the parallel activation of WNT, PI3K–AKT–mTOR and MAPK signalling has its synergistic effect by relieving multiple negative feedback loops and crosstalk between the pathways.

Discussion

Although the androgen signalling pathway and ADT are pivotal in the treatment of advanced PCa, men still relapse with CRPC. Given the importance of feedback in signalling networks, it is important to understand the potential outcomes of crosstalk between key signalling modules in the prostate and possible implications for CRPC. For example, androgen depletion leads to PI3K–AKT pathway stimulation [39] and increased nuclear co-localization and interaction of endogenous AR and β-catenin [40]. Our study provides evidence of clear synergistic crosstalk between the WNT, PI3K–AKT and MAPK signalling pathways driving progression in prostate tumourigenesis.

Transcriptional alterations in both PI3K–AKT and MAPK are common in PCa, particularly in metastatic tumours [1]. These two pathways are regulated by a number of types of crosstalk, including both activating and inhibitory loops [41]. RAS can directly bind to and activate PI3K [42]. TSC1/2, which is a key suppressor of PI3K-dependent stimulation of mTORC1 [43], can be inhibited by oncogenic MAPK signalling through both ERK and ribosomal S6 kinase (RSK)-dependent phosphorylation, resulting in increased mTORC1 signalling [44]. Furthermore, both ERK [44] and RSK [45,46] have been shown to directly phosphorylate raptor to enhance mTORC1 activity. AKT negatively regulates ERK activation by phosphorylating inhibitory sites in the RAF N-terminus [47], ERK phosphorylation inhibits RAF and MEK [48], and phosphorylation of the downstream mTORC1 effector S6 K feeds back to inhibit AKT activity and, in turn, mTORC1 signalling [49]. mTORC1 inhibition, in turn, activates MAPK signalling through a PI3K-dependent feedback loop [50]. We illustrate the multitude of regulatory links between PI3K–AKT and MAPK in supplementary material, Figure S9.

Complex interactions between androgen depletion and the PI3K–AKT–mTOR and MAPK pathways have therapeutic implications. mTORC1 signalling is emerging as a key pathway that directs ADT resistance and stimulates tumour growth in the setting of castrate levels of testosterone (CRPC) [51]. The importance of mTORC1 signalling has resulted in the development of inhibitors such as rapamycin and its analogues, including everolimus and temsirolimus. Early studies with these inhibitors in PCa demonstrated regression of prostate intraepithelial neoplasia lesions in a mouse model overexpressing AKT [52], and inhibition of growth of xenograft models derived from human cells lines with *PTEN* loss [53]. Despite these promising preclinical results and the success of mTORC1 inhibitors in the treatment of patients with metastatic renal cell carcinoma [54], the clinical use of mTORC1 inhibitors in men with metastatic PCa has been disappointing. Phase I/II trials using single agents such as rapamycin or everolimus have failed to show anti-tumour effects, with little effect on prostate-specific antigen or clinical progression [55,56]. The lack of therapeutic effects can be ascribed to MAPK pathway activation through a PI3K-dependent feedback loop in prostate tumours of patients treated with mTOR inhibitors [50]. Dual PI3K/mTORC1/2 drugs such as BEZ235 (Novartis) have shown positive effects in overcoming docetaxel resistance in preclinical studies [57] and in mouse xenograft models [58]. Although the use of BEZ235 for the treatment of PCa has been discontinued, the results have stimulated a search for agents targeting PI3K–AKT–mTOR signalling with a more favourable therapeutic index [59].

WNT signalling can integrate with both the PI3K–AKT–mTOR and MAPK pathways either directly via the GSK3β–TSC2 axis or indirectly via β-catenin-dependent canonical WNT signalling, stimulation of *c-Myc* transcription and inhibition of MAPK-stimulated senescence pathways (supplementary material, Figure S9) [60,61], or β-catenin interactions with AR [40]. In the absence of a WNT signal, GSK3β phosphorylates β-catenin as part of the destruction complex. When WNT signalling is activated, GSK3β is sequestered in multivesicular endosomes, allowing β-catenin to accumulate [62]. GSK3β can also phosphorylate TSC2 and promote TSC1/2 activity, so WNT-dependent inhibition of GSK3β may stimulate both mTOR signalling and canonical WNT pathway activation [60].

Furthermore, phosphorylation of GSKβ by AKT or ERK can also result in TSC1/2 activation [36] or β-catenin-dependent WNT signalling [61], respectively.

GSK3β is known to interact with p53 [63], and p53 is implicated in negative feedback loops controlling cell growth by restraining WNT signalling [34]. In some models, *Pten*-deficient mouse prostates show activated p53 and senescence [64], and the RAS–RAF axis also can stimulate p16/p21/p53-dependent senescence in a variety of tissues [65]. Consistent with the convergence of these three pathways on mTORC1, and the feedback loops and crosstalk regulating them, only simultaneous deregulation of the PI3K, WNT and MAPK pathways resulted in significantly elevated mTORC1 signalling in our mouse models.

Importantly, in our models, canonical WNT signalling was activated at the level of β-catenin, not further up the pathway, e.g. by deletion of APC [30,66]. Collapse of the β-catenin destruction complex following APC loss will not only lead to β-catenin stabilization, but may also free GSK3β to phosphorylate targets such as TSC2. In our system, the presence of activated β-catenin was sufficient to drive synergistic crosstalk with the PI3K–AKT and MAPK pathways. This has allowed us to isolate the specific role of β-catenin transcriptional activity.

Our findings are consistent with previous studies using similar animal models with single or double conditional alleles. However, we do see some differences. Some authors have reported senescence in models in which *Pten* alone was knocked out in a prostate-specific manner [18,64]; however, this is not true of all models [15], and we did not observe this. The differences may be due to background strain or the particular conditional allele being used. As previous authors reported [15], combined β-catenin activation and *Pten* deletion led to accelerated tumour growth, increased invasive ability, and squamous differentiation. We found one incidence of metastasis with this combination, unlike a previous study [15], in which no indication of metastases was found, but in which mice were culled at an earlier age than in our study. Activated β-catenin is likely to drive proliferation of invading cells and primary tumour growth, but not metastasis as such, leading to death from primary tumour morbidity. The one $Catnb^{+/ex3}Pten^{fl/fl}$ mouse showing a metastasis is likely to have resulted from a chance combination of rapid invasion of tumour cells with a longer lifespan.

We observed greater metastatic incidence in $Pten^{fl/fl}K\text{-}Ras^{+/V12}$ mice than in $Catnb^{+/ex3}Pten^{fl/fl}$ mice. $Pten^{fl/fl}K\text{-}Ras^{+/V12}$ mice had longer survival than mice with the more aggressive $Pten^{fl/fl}K\text{-}Ras^{+/D12}$ combination described previously [16], but, consistent with our findings, macrometastatic lesions were reported in all $Pten^{fl/fl}K\text{-}Ras^{+/D12}$ and $Pten^{fl/+}K\text{-}Ras^{+/D12}$ mice. The more extensive nature of the metastases and their rapid development is likely to have resulted from the use of the more aggressive $K\text{-}Ras^{+/D12}$ allele. Interestingly, some evidence of the presence of recombined alleles was detected in bone, but overt bone metastases were not observed [16]. In a PCa model in which *Cre* was driven from a knock-in to the *Nkx3.1* promoter, the combination of $BRAF^{V600E}$ activation with *Pten* deletion resulted in animal lethality comparable to that induced by $Pten^{fl/fl}K\text{-}Ras^{+/D12}$, with an extensive metastatic burden, and was associated with elevated c-MYC activity [17]. In contrast to both our observations on $K\text{-}Ras^{+/V12}$ and previous data on $K\text{-}Ras^{+/D12}$ [16], activation of $BRAF^{V600E}$ alone stimulated cell proliferation [17]. Importantly, however, NKX3.1 is a negative regulator of c-MYC transcriptional activity, and the *Nkx3.1-Cre* knock-in has a haploinsufficient phenotype with elevated basal levels of c-MYC activity [67]. Analysis of this model is therefore confounded by use of the *Nkx3.1-Cre* knock-in and the role of c-MYC, which may be mimicking, at least partly, activated β-catenin. Nevertheless, although mutant BRAF and KRAS belong to the same signalling axis, the differences between the models suggest that the activation of BRAF and the activation of KRAS have different implications, particularly for proliferation. Taken together, these studies imply a distinct role for KRAS activation combined with *Pten* deletion in promoting prostate metastasis. It is likely that the reason why we did not observe metastasis in our triple mutant model is simply that the mice succumbed so rapidly to the growth of the primary tumour.

Our study has limitations. The differences in prostate anatomy between mouse and human mean that the interactions of mouse prostate tissue with the microenvironment may be different between the species (and, indeed, different in different lobes), affecting neoplastic processes. More importantly, the main cause of death in humans with PCa is metastasis, typically to the bone, whereas mouse models of PCa need to be euthanized as a result of locally advanced tumours. Indeed, despite increased PI3K, WNT, MAPK and mTORC1 signalling, triple mutant mice did not develop lymph node metastases. This is probably due to the rapid progression of the primary tumour not allowing the necessary time for metastases to develop. In one model, $Pten^{fl/fl}K\text{-}Ras^{+/V12}$, >50% of mice did develop lymph node metastases, consistent with previous reports [16]. However, they still had to be euthanized as a result of locally advanced prostate tumours. It is unclear whether, even in the models that show lymph node metastasis, dissemination to organs or bone would ever happen. There are few autochthonous mouse models of any cancer driven by genetic lesions mimicking human disease that spontaneously develop overt bone metastases, although SV40 T-antigen models can do so [68], and, in $Pten^{fl/fl}K\text{-}Ras^{+/D12}$ mice, recombined cells were detected in bone [16]. Therefore, there remains a lack of mouse models that truly mimic advanced PCa.

In summary, we have shown that the PI3K, WNT and MAPK signalling pathways cooperate to accelerate prostate tumourigenesis and activate mTORC1 signalling, one of the key drivers of resistance to ADT. Our findings suggest that, in addition to PI3K pathway inhibition, AR inhibitors could be combined with either MAPK or WNT pathway inhibitors with therapeutic benefit in CRPC. However, although mTORC1 may be difficult to activate as a result of dysregulation of a single

pathway, once activated it may require intervention of more than one pathway to inhibit its activity, or indeed to prevent feedback loops from activating other oncogenic pathways [50]. Our triple mutant mouse model provides an excellent system for preclinical studies of multiple pathway inhibition as a therapeutic approach to targeting mTOR.

Acknowledgements

This work was supported by Prostate Cancer UK via a Movember Project Grant (PG12-16). BYS is supported by the Prostate Cancer Research Centre and the European Cancer Stem Cell Research Institute. VM is supported by Cancer Research Wales. MJS is supported by Cancer Research UK. The authors would like to thank Dr Andrew Tee for his critical reading of the manuscript. This manuscript is dedicated to the memory of the late Alan R. Clarke.

Author contributions statement

The authors contributed in the following way: MTJ, ACC, HGK, ARC: study concept and design; ARC, HGK: study supervision; MTJ, BYS, ARC, MJS: drafting of the manuscript. All authors: acquisition and analysis of data. All authors other than ARC gave final approval to the submitted and published versions.

References

1. Taylor BS, Schultz N, Hieronymus H, *et al.* Integrative genomic profiling of human prostate cancer. *Cancer Cell* 2010; **18:** 11–22.
2. Berger MF, Lawrence MS, Demichelis F, *et al.* The genomic complexity of primary human prostate cancer. *Nature* 2011; **470:** 214–220.
3. Barbieri CE, Baca SC, Lawrence MS, *et al.* Exome sequencing identifies recurrent SPOP, FOXA1 and MED12 mutations in prostate cancer. *Nat Res* 2012; **44:** 685–689.
4. Baca SC, Prandi D, Lawrence MS, *et al.* Punctuated evolution of prostate cancer genomes. *Cell* 2013; **153:** 666–677.
5. Tomlins SA, Rhodes DR, Perner S, *et al.* Recurrent fusion of TMPRSS2 and ETS transcription factor genes in prostate cancer. *Science* 2005; **310:** 644–648.
6. Kumar A, White TA, MacKenzie AP, *et al.* Exome sequencing identifies a spectrum of mutation frequencies in advanced and lethal prostate cancers. *Proc Natl Acad Sci U S A* 2011; **108:** 17087–17092.
7. Grasso CS, Wu Y-M, Robinson DR, *et al.* The mutational landscape of lethal castration-resistant prostate cancer. *Nature* 2012; **487:** 239–243.
8. Rajan P, Sudbery IM, Villasevil MEM, *et al.* Next-generation sequencing of advanced prostate cancer treated with androgen-deprivation therapy. *Eur Urol* 2014; **66:** 32–39.
9. Beltran H, Yelensky R, Frampton GM, *et al.* Targeted next-generation sequencing of advanced prostate cancer identifies potential therapeutic targets and disease heterogeneity. *Eur Urol* 2013; **63:** 920–926.
10. Robinson D, Van Allen EM, Wu Y-M, *et al.* Integrative clinical genomics of advanced prostate cancer. *Cell* 2015; **161:** 1215–1228.
11. Giles RH, van Es JH, Clevers H. Caught up in a Wnt storm: Wnt signaling in cancer. *Biochim Biophys Acta* 2003; **1653:** 1–24.
12. Mukherjee R, McGuinness DH, McCall P, *et al.* Upregulation of MAPK pathway is associated with survival in castrate-resistant prostate cancer. *Br J Cancer* 2011; **104:** 1920–1928.
13. Pearson HB, Phesse TJ, Clarke AR. K-ras and Wnt signaling synergize to accelerate prostate tumorigenesis in the mouse. *Cancer Res* 2009; **69:** 94–101.
14. Carstens JL, Shahi P, Van Tsang S, *et al.* FGFR1–WNT–TGF-β signaling in prostate cancer mouse models recapitulates human reactive stroma. *Cancer Res* 2014; **74:** 609–620.
15. Francis JC, Thomsen MK, Taketo MM, *et al.* β-catenin is required for prostate development and cooperates with Pten loss to drive invasive carcinoma. *PLoS Genet* 2013; **9:** e1003180.
16. Mulholland DJ, Kobayashi N, Ruscetti M, *et al.* Pten loss and RAS/MAPK activation cooperate to promote EMT and metastasis initiated from prostate cancer stem/progenitor cells. *Cancer Res* 2012; **72:** 1878–1889.
17. Wang J, Kobayashi T, Floc'h N, *et al.* B-Raf activation cooperates with PTEN loss to drive c-Myc expression in advanced prostate cancer. *Cancer Res* 2012; **72:** 4765–4776.
18. Ahmad I, Patel R, Singh LB, *et al.* HER2 overcomes PTEN (loss)-induced senescence to cause aggressive prostate cancer. *Proc Natl Acad Sci U S A* 2011; **108:** 16392–16397.
19. Patel R, Gao M, Ahmad I, *et al.* Sprouty2, PTEN, and PP2A interact to regulate prostate cancer progression. *J Clin Invest* 2013; **123:** 1157–1175.
20. Sansom OJ, Meniel VS, Muncan V, *et al.* Myc deletion rescues Apc deficiency in the small intestine. *Nature* 2007; **446:** 676–679.
21. Kilkenny C, Browne WJ, Cuthill IC, *et al.* Improving bioscience research reporting: the ARRIVE guidelines for reporting animal research. *PLoS Biol* 2010; **8:** e1000412.
22. Harada N, Tamai Y, Ishikawa T, *et al.* Intestinal polyposis in mice with a dominant stable mutation of the beta-catenin gene. *EMBO J* 1999; **18:** 5931–5942.
23. Guerra C, Mijimolle N, Dhawahir A, *et al.* Tumor induction by an endogenous K-ras oncogene is highly dependent on cellular context. *Cancer Cell* 2003; **4:** 111–120.
24. Suzuki A, Yamaguchi MT, Ohteki T, *et al.* T cell-specific loss of Pten leads to defects in central and peripheral tolerance. *Immunity* 2001; **14:** 523–534.
25. Wu X, Wu J, Huang J, *et al.* Generation of a prostate epithelial cell-specific Cre transgenic mouse model for tissue-specific gene ablation. *Mech Dev* 2001; **101:** 61–69.
26. Ittmann M, Huang J, Radaelli, *et al.* Animal models of human prostate cancer: The Consensus Report of the New York Meeting of the Mouse Models of Human Cancers Consortium Prostate Pathology Committee. *Cancer Res* 2013; **73:** 2718–2736.
27. Wang S, Gao J, Lei Q, *et al.* Prostate-specific deletion of the murine Pten tumor suppressor gene leads to metastatic prostate cancer. *Cancer Cell* 2003; **4:** 209–221.
28. Gounari F, Signoretti S, Bronson R, *et al.* Stabilization of beta-catenin induces lesions reminiscent of prostatic intraepithelial neoplasia, but terminal squamous transdifferentiation of other secretory epithelia. *Oncogene* 2002; **21:** 4099–4107.
29. Bierie B, Nozawa M, Renou J-P, *et al.* Activation of beta-catenin in prostate epithelium induces hyperplasias and squamous transdifferentiation. *Oncogene* 2003; **22:** 3875–3887.
30. Bruxvoort KJ, Charbonneau HM, Giambernardi TA, *et al.* Inactivation of Apc in the mouse prostate causes prostate carcinoma. *Cancer Res* 2007; **67:** 2490–2496.
31. Bjerke GA, Pietrzak K, Melhuish TA, *et al.* Prostate cancer induced by loss of Apc is restrained by TGFβ signaling. *PLoS ONE* 2014; **9:** e92800.

32. Orsulic S, Huber O, Aberle H, *et al.* E-cadherin binding prevents beta-catenin nuclear localization and beta-catenin/LEF-1-mediated transactivation. *J Cell Sci* 1999; **112:** 1237–1245.
33. Reed KR, Meniel VS, Marsh V, *et al.* A limited role for p53 in modulating the immediate phenotype of Apc loss in the intestine. *BMC Cancer* 2008; **8:** 162.
34. Kim NH, Kim HS, Kim N-G, *et al.* p53 and microRNA-34 are suppressors of canonical Wnt signaling. *Sci Signal* 2011; **4:** ra71.
35. Cross DA, Alessi DR, Cohen P, *et al.* Inhibition of glycogen synthase kinase-3 by insulin mediated by protein kinase B. *Nature* 1995; **378:** 785–789.
36. McManus EJ, Sakamoto K, Armit LJ, *et al.* Role that phosphorylation of GSK3 plays in insulin and Wnt signalling defined by knockin analysis. *EMBO J* 2005; **24:** 1571–1583.
37. Cirit M, Wang C-C, Haugh JM. Systematic quantification of negative feedback mechanisms in the extracellular signal-regulated kinase (ERK) signaling network. *J Biol Chem* 2010; **285:** 36736–36744.
38. Ruvinsky I, Sharon N, Lerer T, *et al.* Ribosomal protein S6 phosphorylation is a determinant of cell size and glucose homeostasis. *Genes Dev* 2005; **19:** 2199–2211.
39. Carver BS, Chapinski C, Wongvipat J, *et al.* Reciprocal feedback regulation of PI3K and androgen receptor signaling in PTEN-deficient prostate cancer. *Cancer Cell* 2011; **19:** 575–586.
40. Wang G, Wang J, Sadar MD. Crosstalk between the androgen receptor and beta-catenin in castrate-resistant prostate cancer. *Cancer Res* 2008; **68:** 9918–9927.
41. Mendoza MC, Er EE, Blenis J. The Ras–ERK and PI3K–mTOR pathways: cross-talk and compensation. *Trends Biochem Sci* 2011; **36:** 320–328.
42. Suire S, Hawkins P, Stephens L. Activation of phosphoinositide 3-kinase gamma by Ras. *Curr Biol* 2002; **12:** 1068–1075.
43. Manning BD, Tee AR, Logsdon MN, *et al.* Identification of the tuberous sclerosis complex-2 tumor suppressor gene product tuberin as a target of the phosphoinositide 3-kinase/akt pathway. *Mol Cell* 2002; **10:** 151–162.
44. Carriere A, Romeo Y, Acosta-Jaquez HA, *et al.* ERK1/2 phosphorylate Raptor to promote Ras-dependent activation of mTOR complex 1 (mTORC1). *J Biol Chem* 2011; **286:** 567–577.
45. Roux PP, Ballif BA, Anjum R, *et al.* Tumor-promoting phorbol esters and activated Ras inactivate the tuberous sclerosis tumor suppressor complex via p90 ribosomal S6 kinase. *Proc Natl Acad Sci U S A* 2004; **101:** 13489–13494.
46. Carriere A, Cargnello M, Julien L-A, *et al.* Oncogenic MAPK signaling stimulates mTORC1 activity by promoting RSK-mediated raptor phosphorylation. *Curr Biol* 2008; **18:** 1269–1277.
47. Zimmermann S, Moelling K. Phosphorylation and regulation of Raf by Akt (protein kinase B). *Science* 1999; **286:** 1741–1744.
48. Dhillon AS, Hagan S, Rath O, *et al.* MAP kinase signalling pathways in cancer. *Oncogene* 2007; **26:** 3279–3290.
49. Dibble CC, Asara JM, Manning BD. Characterization of Rictor phosphorylation sites reveals direct regulation of mTOR complex 2 by S6K1. *Mol Cell Biol* 2009; **29:** 5657–5670.
50. Carracedo A, Ma L, Teruya-Feldstein J, *et al.* Inhibition of mTORC1 leads to MAPK pathway activation through a PI3K-dependent feedback loop in human cancer. *J Clin Invest* 2008; **118:** 3065–3074.
51. Edlind MP, Hsieh AC. PI3K–AKT–mTOR signaling in prostate cancer progression and androgen deprivation therapy resistance. *Asian J Androl* 2014; **16:** 378–386.
52. Majumder PK, Febbo PG, Bikoff R, *et al.* mTOR inhibition reverses Akt-dependent prostate intraepithelial neoplasia through regulation of apoptotic and HIF-1-dependent pathways. *Nat Med* 2004; **10:** 594–601.
53. Wu L, Birle DC, Tannock IF. Effects of the mammalian target of rapamycin inhibitor CCI-779 used alone or with chemotherapy on human prostate cancer cells and xenografts. *Cancer Res* 2005; **65:** 2825–2831.
54. Motzer RJ, Escudier B, Oudard S, *et al.* Efficacy of everolimus in advanced renal cell carcinoma: a double-blind, randomised, placebo-controlled phase III trial. *Lancet* 2008; **372:** 449–456.
55. Templeton AJ, Dutoit V, Cathomas R, *et al.* Phase 2 trial of single-agent everolimus in chemotherapy-naive patients with castration-resistant prostate cancer (SAKK 08/08). *Eur Urol* 2013; **64:** 150–158.
56. Amato RJ, Jac J, Mohammad T, *et al.* Pilot study of rapamycin in patients with hormone-refractory prostate cancer. *Clin Genitourin Cancer* 2008; **6:** 97–102.
57. Antonarakis ES, Armstrong AJ. Evolving standards in the treatment of docetaxel-refractory castration-resistant prostate cancer. *Prostate Cancer Prostatic Dis* 2011; **14:** 192–205.
58. Yasumizu Y, Miyajima A, Kosaka T, *et al.* Dual PI3K/mTOR inhibitor NVP-BEZ235 sensitizes docetaxel in castration resistant prostate cancer. *J Urol* 2014; **191:** 227–234.
59. Wei XX, Hsieh AC, Kim W, *et al.* A Phase I study of abiraterone acetate combined with BEZ235, a dual PI3K/mTOR inhibitor, in metastatic castration resistant prostate cancer. *Oncologist* 2017; **22:** 503–543.
60. Inoki K, Ouyang H, Zhu T, *et al.* TSC2 integrates Wnt and energy signals via a coordinated phosphorylation by AMPK and GSK3 to regulate cell growth. *Cell* 2006; **126:** 955–968.
61. Ding Q, Xia W, Liu J-C, *et al.* Erk associates with and primes GSK-3beta for its inactivation resulting in upregulation of beta-catenin. *Mol Cell* 2005; **19:** 159–170.
62. Taelman VF, Dobrowolski R, Plouhinec J-L, *et al.* Wnt signaling requires sequestration of glycogen synthase kinase 3 inside multivesicular endosomes. *Cell* 2010; **143:** 1136–1148.
63. Watcharasit P, Bijur GN, Zmijewski JW, *et al.* Direct, activating interaction between glycogen synthase kinase-3beta and p53 after DNA damage. *Proc Natl Acad Sci U S A* 2002; **99:** 7951–7955.
64. Chen Z, Trotman LC, Shaffer D, *et al.* Crucial role of p53-dependent cellular senescence in suppression of Pten-deficient tumorigenesis. *Nature* 2005; **436:** 725–730.
65. Collado M, Serrano M. Senescence in tumours: evidence from mice and humans. *Nat Rev Cancer* 2010; **10:** 51–57.
66. Valkenburg KC, Hostetter G, Williams BO. Concurrent Hepsin overexpression and adenomatous polyposis coli deletion causes invasive prostate carcinoma in mice. *Prostate* 2015; **75:** 1579–1585.
67. Anderson PD, McKissic SA, Logan M, *et al.* Nkx3.1 and Myc crossregulate shared target genes in mouse and human prostate tumorigenesis. *J Clin Invest* 2012; **122:** 1907–1919.
68. Klezovitch O, Chevillet J, Mirosevich J, *et al.* Hepsin promotes prostate cancer progression and metastasis. *Cancer Cell* 2004; **6:** 185–195.

SUPPLEMENTARY MATERIAL ONLINE.

Supplementary materials and methods.

Supplementary figure legends.

Figure S1. Histological characterisation of invasive adenocarcinoma, reactive stroma and squamous metaplasia in *Catnb*$^{+/ex3}$ *Pten*$^{fl/fl}$ *K-Ras*$^{+/V12}$ triple mutant prostate tumours

Figure S2. Percentage of invasive adenocarcinoma

Figure S3. Rate of growth of prostate tumours

Figure S4. Proliferation of prostatic lesions by Ki67 and BrdU staining

Figure S5. Rate of apoptosis according to percentage (%) of Caspase-3 positivity at endpoint (500 days or when sick)

Figure S6. Immunohistochemistry for p-GSKβ^{Ser9} for all mouse models

Figure S7. Immunohistochemistry for p-ERK 1/2 for all mouse models

Figure S8. Biochemical analysis of signalling pathways in wild type and single allele prostate tissue

Figure S9. Complex interactions between PI3K, Wnt and MAPK pathways resulting in aberrant mTORC1 signalling

Table S1. Percentages of animals with nodal metastasis

Table S2. Full statistical comparisons (unpaired t-tests, n = 3) for Quickscore quantitations